Research Article | Vol. 10, No. 10 / 1 October 2020 / Optical Materials Express 2345
Optical Materials EXPRESS

Tailored nanocomposites for 3D printed micro-optics

Ksenia Weber,[1] Daniel Werdehausen,[2,3] Peter König,[4] Simon Thiele,[5] Michael Schmid,[1] Manuel Decker,[2] Peter William De Oliveira,[4] Alois Herkommer,[5] and Harald Giessen[1,*]

[1]4th Physics Institute and Research Center SCoPE, University of Stuttgart, Pfaffenwaldring 57, 70569 Stuttgart, Germany
[2]Corporate Research & Technology, Carl Zeiss AG, Carl Zeiss Promenade 10, 07745 Jena, Germany
[3]Institute of Applied Physics, Abbe Center of Photonics, Friedrich Schiller University Jena, Albert-Einstein-Str. 15, 07745 Jena, Germany
[4]INM - Leibniz Institute for New Materials, 66123 Saarbrücken, Germany
[5]Institute of Applied Optics (ITO) and Research Center SCoPE, University of Stuttgart, Pfaffenwaldring 9, 70569 Stuttgart, Germany
*h.giessen@pi4.uni-stuttgart.de

Abstract: Optical polymers cover only a rather narrow range of optical properties. This is a limiting factor for the design of polymer-based optical systems such as smartphone cameras. Moreover, it also poses a problem for femtosecond two-photon lithography, which is a state-of-the-art technology to 3D print high-quality optics from photopolymers. To overcome the limitations of conventional polymers, we introduce nano-inks based on the commonly used photopolymers IP-DIP and IP-S as polymer matrix and zirconium dioxide (ZrO_2) nanoparticles. We show that the refractive index and dispersion of these nano-inks can be purposefully tailored by varying the constituent materials and the volume fraction of the nanoparticles. Furthermore, we demonstrate the suitability of our nano-inks for optical applications by 3D printing single micro-lenses and a multi-material achromatic Fraunhofer doublet. Our findings confirm that nanocomposites expand the range of optical properties that are accessible for polymer-based systems and allow for the design of tailored optical materials.

1. Introduction

In optical design, the use of materials spanning a wide range of optical properties is a powerful tool for correcting both chromatic and monochromatic aberrations [1]. Therefore, such materials are a key ingredient of high-performance optical systems [2]. The quantities that are commonly used to quantify the optical properties of a material are the refractive index at the d-line $n_d = n(\lambda_d = 587.56\ \text{nm})$ and the Abbe number $\nu_d = (n_d - 1)/(n_F - n_C)$, where the subscripts F, d, C refer to the Fraunhofer spectral lines at $\lambda_F = 486.13$ nm, $\lambda_d = 587.56$ nm, and $\lambda_C = 656.28$ nm [1]. These definitions indicate that n_d denotes the overall magnitude of the refractive index, whereas ν_d quantifies its dispersion. In fact, many key scientific and industrial advances in the 19th and 20th centuries, for example high-resolution microscopes, were enabled by the development of high-quality optical glasses which cover a wide range of n_d and ν_d values [2]. To visualize the range that is encompassed by optical glasses today, the green area in Fig. 1(a) highlights the region in the Abbe diagram that is covered by the current Schott glass catalog [3]. In contrast, many modern optical systems, especially compact consumer devices like smartphone cameras, rely on optical polymers. This is because of their low weight, low price, high impact resistance, and good manufacturability [4]. Furthermore, a key technology that inherently relies on optical polymers is femtosecond two-photon direct laser writing. In recent

#399392 https://doi.org/10.1364/OME.399392
Journal © 2020 Received 4 Jun 2020; revised 4 Aug 2020; accepted 4 Aug 2020; published 2 Sep 2020

Optical Materials EXPRESS

years, this technique has become an enabling technology for 3D printing high-performance optics on length scales between micro- and millimeters [5–14]. In contrast to classical lens grinding methods, this approach allows for producing free-form surfaces without any additional costs [15–17]. This allows for an enormous optical design freedom. However, all optical systems and technologies that rely on optical polymers suffer from the fact that polymers only cover a narrow range of optical properties. Specifically, as visualized by the blue area in Fig. 1(a), polymers are restricted to much smaller refractive indices than optical glasses [4,18,19]. This is a limiting factor for the design of optical systems relying on polymers, e.g. those that are manufactured by techniques such as femtosecond two-photon direct laser writing [20–22]. A promising approach to overcome these limitations is incorporating nanoparticles made of high-refractive-index dielectric materials into a polymer as host matrix [23–25]. As visualized in Figs. 1(b) and 1(c), the much higher effective refractive index of such nanocomposites compared to conventional polymers, for example allows for increasing the performance of a lens while simultaneously decreasing its size. In fact, a recent general analysis based on the Maxwell-Garnett-Mie effective medium theory [24–26] has proposed that nanocomposites could serve as a platform of next-generation optical materials that allows for tailoring *both the magnitude and the dispersion* of the effective refractive index within wide regions [23]. However, so far, experimental research into high-refractive-index nanocomposites was mostly restricted to thin coatings that can, for

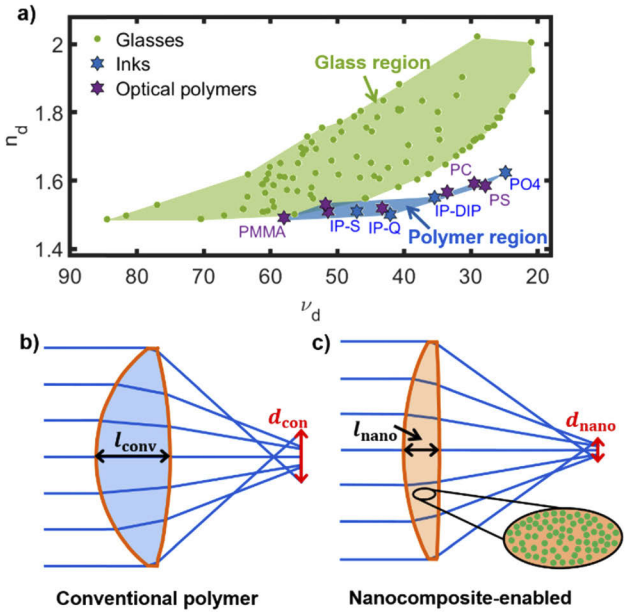

Fig. 1. (a) Abbe diagram (refractive index at the d-line $n_d = n(\lambda_d = 587.56\,\text{nm})$ over the Abbe number ν_d) including photoresists (inks) for femtosecond 3D printing [21], conventional optical polymers, and the glasses of the Schott glass catalog. The shaded areas show that polymers only cover a narrow range of optical properties, whereas glasses cover a much wider range. From left to right, the conventional polymers (purple stars) included in the figure are: PMMA, COP, Optorez, Styrene, SAN, PC, and PS. (b,c) Layout of a (b) conventional polymer lens and (c) a nanocomposite-enabled lens. Both lenses were designed in "OpticStudio". The blue lines visualize the propagation of rays through the lenses. The nanocomposite-enabled lens is both thinner ($l_{nano} < l_{conv}$) and enables a higher performance ($d_{nano} < d_{conv}$) than the conventional lens. In these figures, d_{conv} and d_{nano} visualize the root mean square (RMS) spot size in the focal plane that can obtained from the ray traces.

Optical Materials EXPRESS

example, be used to increase the extraction efficiencies of LEDs [25,27,28]. The suitability of nanocomposites as a material platform for optical elements and systems has not yet been experimentally demonstrated. Furthermore, the accuracy of the Maxwell-Garnett-Mie effective medium theory for predicting the effective refractive index and its dispersion has never been systematically investigated in experimental works. This is a key issue, because, theoretically, an infinite variety of nanocomposites exist and validated effective medium theories are consequently essential to guide the design of the most promising novel materials.

In this paper, we demonstrate the suitability of nanocomposites as a platform of tailorable materials for optical elements and systems. To this end, we focus on photoresists ("inks") which can be used for femtosecond two-photon direct laser writing. We chose this technology because it enables rapid prototyping and is thus perfectly suited for a proof-of-concept. Furthermore, since the number of available photoresists is currently highly limited, novel tailored materials offer a high potential for this technology. In addition, we also use our nano-inks to systematically investigate the accuracy of the Maxwell-Garnett-Mie effective medium theory for different materials. Finally, we discuss what further steps are required to unlock the full potential of nanocomposites as next-generation optical materials and highlight that nano-inks are also promising materials for other applications.

2. The Maxwell-Garnett-Mie effective medium theory

In this paper, we investigate nanocomposites which are composed of discrete nanoparticles that are embedded into a polymer host matrix. The natural starting point to analytically determine the effective permittivity (ϵ_{eff}) of such materials is the Clausius-Mossotti equation. This equation treats the nanoparticles as polarizable entities with an electric dipole polarizability of α_{inc} and reads [29]:

$$\epsilon_{\text{eff}} = \epsilon_{\text{h}} \frac{1 + \frac{2}{3} N \pi \alpha_{\text{inc}}}{1 - \frac{2}{3} N \pi \alpha_{\text{inc}}}, \tag{1}$$

where ϵ_{h} is the permittivity of the host matrix and N is the nanoparticles' number density. For spherical nanoparticles, the nanoparticles' dipole polarizability that appears in the Clausius-Mossotti equation can be directly determined from Mie theory [30] as follows [26]:

$$\alpha_{\text{inc}} = i \frac{3(d_{\text{inc}}/2)^3}{2x^3} a_1, \tag{2}$$

where a_1 is the first order Mie coefficient, d_{inc} is the diameter of the inclusions, and $\text{x} = \sqrt{\epsilon_{\text{h}}} \pi \text{d}_{\text{scat}} \lambda^{-1}$ is the size parameter [31]. The Maxwell-Garnett-Mie effective medium theory can now readily be obtained by substituting Eq. (2) into Eq. (1). As a more intuitive measure, the volume fraction $\phi = \frac{1}{6} \pi N d_{\text{inc}}^3$ can then be used instead of the number density (N). Finally, if the material's permeability remains negligible, its effective refractive index can be readily determined from $n_{\text{eff}} = \sqrt{\epsilon_{eff}}$.

3. Nanocomposites as tailorable optical materials

To systematically demonstrate that nanocomposites can serve as a platform of novel tailored optical materials, we synthesized four different nano-inks. To this end, we mixed ZrO_2 nanoparticles within a 50 wt.% PGMEA solution (PCPA, Pixelligent) into the two conventional photoresists IP-DIP [$n_d = 1.549$, $\nu_{\text{d}} = 34.98$] [20] and IP-S [$n_d = 1.507$, $\nu_{\text{d}} = 46.16$] [20] (Nanoscribe GmbH) as the host matrices. These photoresists contain a photo-initiator and can consequently be polymerized using ultraviolet (UV) light. Furthermore, the nanoparticles have close to spherical shapes and a narrow size distribution that peaks below a diameter of 10 nm. In addition, the nanoparticles are functionalized to avoid agglomeration in polymers with proprietary capping

Optical Materials EXPRESS

layers that have been disclosed in several patent applications [32–35]. We performed the mixing of the constituent materials in a conical flask under constant stirring with a magnetic mixer.

Subsequently, when homogeneous compounds were formed, we removed the solvent in which the nanoparticles were dispersed by concentrating the mixture under reduced pressure for several hours until the target weight (weight of mixture with all solvent evaporated) was reached. We first performed this process for IP-DIP as the host material and three different volume fractions of nanoparticles. This enables us to systematically analyze the influence of the nanoparticle volume fraction on the optical properties of the nano-inks. In addition, we synthesized a nano-ink based on IP-S as the host matrix to investigate what properties can be achieved by combining different materials. For this nano-ink, we first mixed IP-S with 2-Hydroxy-3-phenoxypropylacrylat (HPPA [$n_d = 1.528$, $\nu_d = 34$]) at a 1:1 ratio to achieve agglomeration-free blending of the nanoparticles in the matrix.

To characterize the optical properties of the nano-inks, we polymerized all materials with UV light and measured their refractive index profile using a commercial automated Pulfrich refractometer [36] (ATR-L, Schmidt and Hänsch GmbH & Co.). Accordingly, Fig. 2(a) displays the dispersion curves of the three IP-DIP based nano-inks and the pure host material, while Fig. 2(b) displays the dispersion curves of the IP-S based nano-ink, pure IP-S and the IP-S/HPPA mixture that was used as the host material. In these figures, the crosses denote the measured data points, whereas the solid line represent Cauchy functions that we fitted to the experimental data. These fits enable us to accurately determine the n_d and ν_d values of all materials from the measured data. In addition, the dashed blue lines in Fig. 2(a) depict the predictions obtained from the EMT. It is evident that there is an excellent agreement between experimental data and theory. Note that we determined the volume fraction of each nano-ink from the EMT. To this end, we used Eq. (1) and Eq. (2) together with the refractive indices of ZrO_2 and the respective host material [20,37]. We then fitted the resulting expression for n_{eff} to our experimental data by using the volume fraction ϕ as the only free parameter. We used this approach because, in practice, the key question is whether the EMT can accurately predict what dispersion properties, that is n_d and ν_d values, can be achieved by varying the volume fractions. To directly visualize the n_d and ν_d values of all nano-inks, Fig. 2(c) depicts their locations in the Abbe diagram (orange stars). This figure indicates that the nano-inks are located well within the region that is normally only accessible using optical glasses. Specifically, Fig. 2 demonstrates that increasing the volume fraction of the nanoparticles systematically increases the magnitude of the refractive index. Furthermore, it is evident that the EMT predicts the n_d and ν_d values that can be achieved by varying the volume fractions with high accuracy. The finding that the refractive index of our nano-inks are much higher than those of the pure host materials shows that our nano-inks indeed overcome the restrictions of conventional polymers that we discussed in the introduction (see Fig. 1(a)). In fact, it is well known from aberration theory [38], that materials of a high refractive index allow for reducing spherical aberration or, in combination with materials with a low refractive index, also allow for reducing the Petzval field curvature [28]. In addition to the IP-DIP based nano-inks, the location of the IP-S based nano-ink in the Abbe diagram in Fig. 2(c) demonstrates that different regions in the Abbe diagram can be accessed by combining different materials. It is evident that the IP-S based nano-ink is characterized by a higher Abbe number than the IP-DIP based nano-inks. In optical design, such materials with higher Abbe numbers are useful for reducing chromatic aberrations [28]. Furthermore, the dashed blue lines in Fig. 2(c), which depict the predictions from the EMT for volume fractions between 0% and 35%, directly show that the EMT accurately predicts the locations of all nano-inks in the Abbe diagram. Specifically, the Abbe numbers of all nano-inks deviate by less than 0.9% from those obtained from the EMT at the same value of n_d. Both our experimental findings and theoretical predictions hence demonstrate that the host matrix and the nanoparticle materials define a trajectory in the Abbe diagram. Adjusting the volume fraction then allows for tuning the

Optical Materials EXPRESS

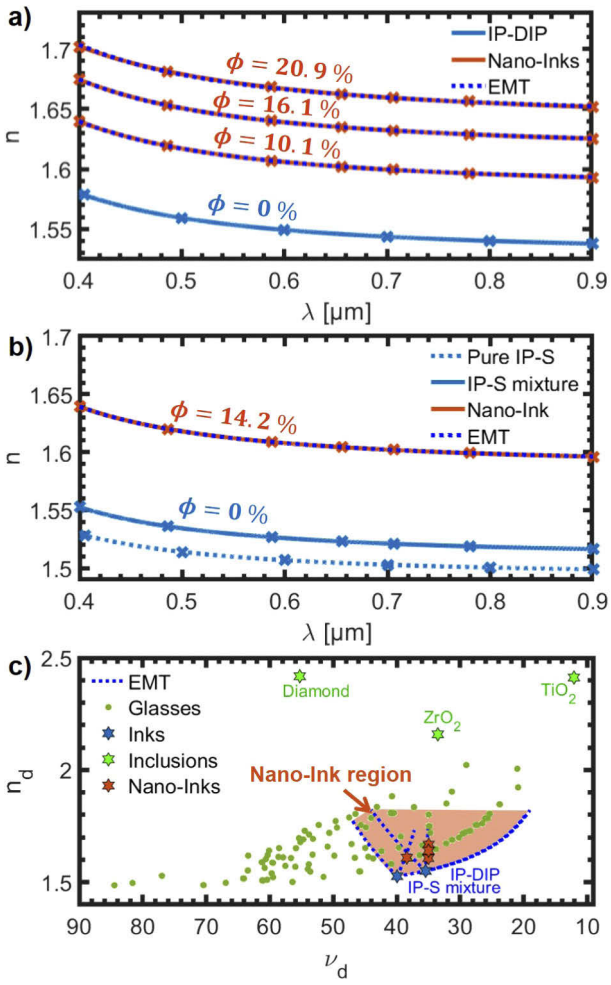

Fig. 2. Refractive index as a function of the wavelength for (a) the three IP-DIP-based nano-inks and (b) nano-ink based on a mixture of IP-S and 2-Hydroxy-3-phenoxypropylacrylat as the host material at different volume fractions Φ of ZrO_2 nanoparticles. The crosses denote the measured data points, the solid lines Cauchy fits, and the dashed lines the prediction of the effective medium theory (EMT). The volume fractions were determined from the EMT. Refractive index data for the pure IP photoresists was taken from Ref. [21]. (c) Locations of different materials in the Abbe diagram ($n_d = n(\lambda_d = 587.56\,\text{nm})$) over Abbe number ν_d). In addition to the IP-DIP-based nano-inks the diagram includes a nano-ink that is based on a mixture of IP-S and 2-Hydroxy-3-phenoxypropylacrylat as the host material ($\Phi = 14.2\%$). The dashed blue lines visualize the prediction from the EMT for a wide range of nano-inks that are composed of IP-DIP as well as the IP-S-mixture as the host materials and diamond, ZrO_2 and TiO_2 as the materials of the nanoparticles. These lines extend up to volume fractions of up to 35%. The shaded red area visualizes the region that is accessible by combining different nanoparticle materials in the same host.

Optical Materials EXPRESS

optical properties of the nano-inks along this trajectory. We chose a maximum volume fraction of 35% for our theoretical predictions because such volume fractions have already been achieved for thin films [27]. In fact, building on the finding that the EMT is highly accurate, we can now use the EMT to investigate what locations in the Abbe diagram can be accessed by using different nanoparticle materials. To do so, the Abbe diagram in Fig. 2(c) also includes diamond and TiO_2 as nanoparticle materials. Accordingly, the corresponding dashed blue lines demonstrate that using these materials allows for accessing widely different regions of the Abbe diagram. This confirms that nanocomposites allow for the design of dispersion-engineered materials. In addition, the shaded red area illustrates that combining multiple nanoparticle materials within the same host allows for continuously tuning n_d and ν_d within wide regions. We obtained this area by generalizing the EMT (Eq. (1)) to two different nanoparticle materials. To this end, we added the term $\frac{2}{3}N_2\pi\alpha_{\mathrm{inc},2}$, where N_2 is the number density and $\alpha_{\mathrm{inc},2}$ the polarizability of the second nanoparticle material, to both the numerator and denominator of Eq. (1). Note that this model generally assumes that all inclusions are randomly dispersed and well-blended into the host matrix [24].

4. 3D printed nanocomposite-enabled optical elements

In order to demonstrate the suitability of nanocomposites as next-generation optical materials for optical elements and systems, we first investigate single plano-convex spherical lenses. To this end, we keep the radius of curvature and the diameter of the lenses fixed at 100µm and 120µm, respectively, and use pure IP-DIP as well as the three IP-DIP based nano-inks as the lens materials. This allows us to systematically investigate whether the imaging behavior of the lenses made from our nano-inks match the measured refractive index profiles. We fabricated all optical components presented in this work with the commercial two-photon femtosecond 3D printer Photonics Profession GT (Nanoscribe GmbH). This system is equipped with a femtosecond (≈100 fs)-pulsed fiber laser (780 nm) operating at a repetition rate of 80 MHz. During the printing process, the laser beam is scanned in lateral direction by two galvometric mirrors at a speed of 45,000 µm/s through a 63x (NA = 1.4) microscope objective. Laser powers between 40 to 45% of the 3D printer's maximum laser power were used for printing the different nano-inks. We fabricated all lenses onto glass substrates in dip-in configuration. Subsequently, we placed the lenses into a developer bath (mr-Dev 600, microresist technology GmbH) for several minutes to remove the unexposed nano-ink material. To visualize the appearance of the lenses, Fig. 3(a) depicts a microscope image of the lens made from the $\Phi = 10.1\%$ IP-DIP based nano-ink.

As the next step, to systematically analyze the properties of all lenses, we recorded images of groups 0 and 1 of a USAF 1951 test target chart through each of the lenses under a microscope. The test target has a size of 15×15 mm and was placed at a distance of 3 cm from the lenses. For all experiments, we illuminated the test chart with a white light halogen lamp (no condenser was used for the illumination). The distance between the test target and the lenses was kept constant at all times. Focusing was performed by simultaneously moving the lens and the test chart with a motorized microscope stage. A CCD camera together with a 20x (NA = 0.45) microscope objective was used to record the images. As illustrated in Fig. 3(b), the sizes of the images decrease with increasing ZrO_2 volume fractions. This can be readily understood from the fact that the magnification $\beta = \frac{y'}{y}$, where y is the size of the object and y' is the size of the image can also be expressed as $\beta = \frac{1}{P \cdot y' - 1}$, where the refractive power (P) of the lens follows from $P = \frac{1}{f}$ (f: focal length). If we now consider that, according to the lens maker's equation for thin plano-convex lenses $\frac{1}{f} = \frac{1}{R}(n_d - 1)$, the refractive power is directly proportional to the refractive index of the lens material ($P(\lambda_\mathrm{d}) \propto n_d$), it directly follows that an increase of the refractive index leads to a reduction of the magnification. In order to confirm this relationship quantitatively, we consequently determined the refractive power of all lenses by measuring their focal lengths using

Optical Materials EXPRESS

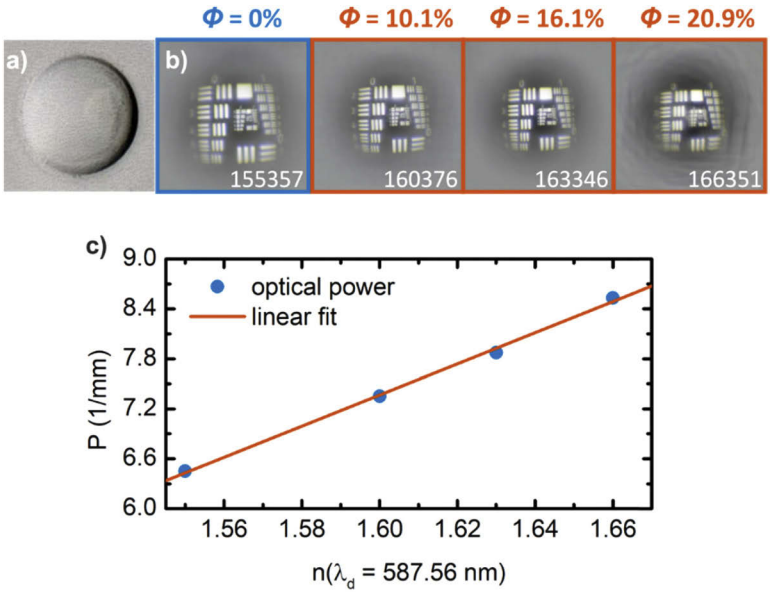

Fig. 3. (a) Exemplary microscope image of the spherical lens made of the $\Phi = 10.1\%$ IP-DIP based nano-ink. (b) Images of a USAF 1951 test target chart obtained through plano-convex spherical lenses with a radius of curvature of 100 µm and a diameter of 120 µm that are composed of the different IP-DIP based nano-inks from Fig. 2. At the bottom of the frame, the equivalent Schott catalog numbers of the different materials are given. (c) Measured optical power ($P = 1/f$) of the micro-lenses in dependence of the refractive index at the d-line (n_d) of the nano-inks. The optical power exhibits the theoretically expected linear behavior.

a mechanical microscope stage. Accordingly, Fig. 3(c) depicts the refractive power of the lenses as a function of their n_d. These data confirm that the refractive power increases linearly with the magnitude of the refractive index of the nano-inks $n(\lambda_d = 587.66)$. This directly demonstrates that nanocomposites can be used as tunable optical materials in optical components. Furthermore, it shows that the 3D printed, two-photon exposed nano-inks exhibit the same behavior as the one-photon exposed nano-inks and the EMT calculations. The EMT can thus be used as a tool to find the optimal material composition already during the design process. Finally, we note that in Fig. 3(b), as opposed to all other lenses, the image of the lens containing the highest concentration of nanoparticles ($\Phi = 20.9\%$) is slightly hazy. This indicates that, in this case, the nanoparticles might no longer be perfectly blended into the polymer matrix.

Finally, since optical systems that achieve aberration-corrected imaging must generally consist of multiple optical elements, we now demonstrate that our nano-inks are also suitable for the fabrication of such multi-element systems. To this end, we use a cemented achromatic Fraunhofer doublet as a prototype system. As illustrated in Fig. 4(a), such an achromat is designed to correct the longitudinal chromatic aberration (LCA) for two selected wavelengths (λ_1 and λ_2). In fact, since LCA is present in all refractive lenses due to the inherent dispersion of optical materials, achromats are also key building blocks of many more complex optical systems. Using the optical design software OpticStudio (ZEMAX), we consequently designed an achromat that is composed of IP-S as well as the IP-S based nano-ink and has a nominal focal length of 3 mm at $\lambda = 500$ nm. As illustrated in the Abbe diagram in Fig. 2(c), this nano-ink exhibits a refractive index at the d-line of $n_d = 1.61$ and an Abbe number of $\nu_d = 38.4$. For the fabrication of this achromat, we used a 25x (NA = 0.8) objective and, first, 3D printed the negative lens onto a glass substrate using the IP-S based nano-ink. We then developed the negative lens and subsequently 3D printed

Optical Materials EXPRESS

the positive lens on top of it using pure IP-S. To visualize the result of this procedure, the inset in Fig. 4(b) presents a photograph of the printed achromat. As a benchmark, we additionally also fabricated a singlet with the same nominal focal length ($f = 3\,\mathrm{mm}$ at $\lambda = 500\,\mathrm{nm}$) from pure IP-S. To ensure the comparability of the two systems, we optimized both the singlet and the achromat optimized for maximum performance using aspherical surfaces.

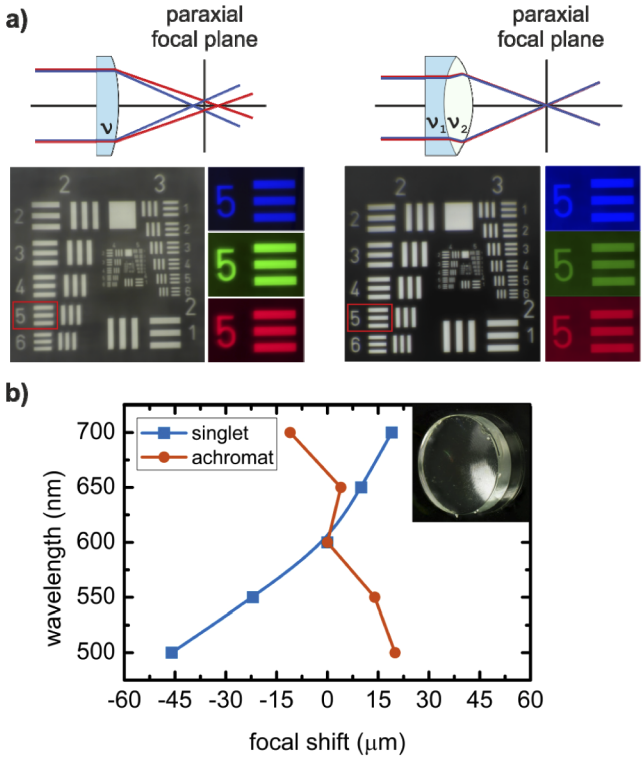

Fig. 4. (a) Ray sketch and imaging of (left) a single lens printed with IP-S and (right) a cemented achromat printed with a combination of IP-S and the IP-S-based nano-ink ($\Phi = 14.2\%$) of the same focal length. Red frames in the white light images highlight the area that is shown on the right-hand side for monochromatic illuminations with different wavelengths (450 nm, 550 nm, and 650 nm). (b) Shift of focal length (in regards to the focal length at 600 nm) at different wavelengths for singlet lens and achromatic Fraunhofer doublet of the same paraxial focal length (3 mm). Solid lines serve as guide to the eye. Inset shows a microscope image of the Fraunhofer doublet.

To directly compare the imaging performance of the achromat and the singlet, Fig. 4(a) again presents images of an USAF 1951 test target chart that we captured through the two devices. As one can see, the image obtained through the achromat exhibits a noticeably increased contrast compared to that obtained through the single lens. This can be attributed to the fact that the achromat is corrected for aberrations to a much higher degree than the single lens. To systematically compare the LCA of the two devices, we consequently inserted bandpass filters with a bandwidth of $\Delta\lambda = 40\,\mathrm{nm}$ into the beam path between the objective and the CCD camera. Accordingly, we obtained the different color images in Fig. 4(a) using a blue filter with a center wavelength of $\lambda_0 = 450\,\mathrm{nm}$, a green filter with $\lambda_0 = 550\,\mathrm{nm}$, and a red filter with $\lambda_0 = 650\,\mathrm{nm}$. These images directly visualize that a defocusing effect can be seen in the images obtained through the singlet lens, whereas this effect is not visible in the images that we recorded through the achromatic doublet. To systematically quantify this effect for both devices, we measured their

Optical Materials EXPRESS

focal shift as a function of the wavelength in the range between 500 nm and 700 nm. For these measurements, we used monochromatic light from a tunable white light laser source and again measured the focal lengths using the mechanical microscope stage. The corresponding data in Fig. 4(c) show a significant reduction of the focus shift for the achromat compared to the singlet lens. Specifically, as expected for an achromat, the focal shift Δf vanishes for two wavelengths. This demonstrates that our nano-inks are also suitable for multi-component optical systems.

5. Conclusion

In this paper, we have experimentally demonstrated that nanocomposites composed of polymers and dielectric nanoparticles can serve as a platform of tailorable materials for optical elements and systems. To this end, we first synthesized and characterized four different nanocomposites that are based on the commonly used photopolymers IP-S and IP-DIP as well as zirconium dioxide (ZrO_2) nanoparticles. Subsequently, we used femtosecond two-photon direct laser writing to 3D print both singlet lenses and a multi-material achromatic doublet from our nanocomposites ("nano-inks"). These devices illustrate that nanocomposites can be used as next-generation optical materials that enable unprecedented design freedom. This is because nanocomposites allow for using not only the surfaces but also the materials themselves as continuous degrees of freedom for the design of optical systems. This holds a high potential for enhancing the performance or reducing the size of optical systems since the aberrations that limit their performance are critically determined by the optical properties of the materials. Furthermore, we used our nano-inks to demonstrate that the Maxwell-Garnett-Mie effective medium theory (EMT) can predict the optical properties of nanocomposites with high accuracy. This finding confirms that this EMT is a powerful tool that allows for finding the optimal materials already in the design process.

To demonstrate the suitability of nanocomposites as next-generation optical materials, we here focused on materials that can be used as photoresists for femtosecond 3D printing, as this technology enables rapid prototyping of micro-optical systems. However, nanocomposites are a highly diverse material class that can potentially offer novel or improved properties for widely different applications, such as smartphone cameras, diffractive optical elements (DOEs) with unpreceded high efficiencies [23,39,40], or even therapeutic materials [41–43]. Our approach of using nanocomposites as nano-inks for femtosecond 3D printing, or other additive manufacturing technologies, could hence provide the basis for a wide range of novel devices. In fact, the idea of using nanocomposites as inks for inkjet printing and stereolithography has already been disclosed in patents and patent applications [44,45].

Funding

Horizon 2020 Framework Programme (675745, NOLOSS); Baden-Württemberg Stiftung (Opterial); European Research Council (AdG COMPLEXPLAS, PoC 3DPRINTEDOPTICS); Bundesministerium für Bildung und Forschung (13N14097, PRINTFUNCTION, PRINTOPTICS, QLinkX).

Acknowledgement

This project has received funding from the European Union's Horizon 2020 research and innovation programme under the Marie Sklodowska-Curie (Grant No. 675745).

Disclosures

The authors declare no conflicts of interest.

References

1. H. Gross, F. Blechinger, and B. Achtner, *Handbook of Optical Systems* (Wiley Online Library, 2005), Vol. 1.

Optical Materials EXPRESS

2. P. Hartmann, R. Jedamzik, S. Reichel, and B. Schreder, "Optical glass and glass ceramic historical aspects and recent developments: a Schott view," Appl. Opt. **49**(16), D157–176 (2010).
3. S. Ag, "*Optical Glass*," https://www.schott.com/d/advanced_optics/c36214d9-13c4-468c-bf40-8d438b89f532/1.14/schott-optical-glass-pocket-catalog-jan-2018-row.pdf.
4. S. Kasarova, N. Sultanova, and I. Nikolov, "Polymer materials in optical design," Bulg. Chem. Commun. **47**, 44–54 (2015).
5. S. Steenhusen, S. Hasselmann, and G. Domann, "Strategies for rapid and reliable fabrication of microoptical structures using two-photon polymerization," in *Advanced Fabrication Technologies for Micro/Nano Optics and Photonics X* (International Society for Optics and Photonics, 2017), Vol. 10115, p. 101150S.
6. S. Thiele, K. Arzenbacher, T. Gissibl, H. Giessen, and A. M. Herkommer, "3D-printed eagle eye: Compound microlens system for foveated imaging," Sci. Adv. **3**(2), e1602655 (2017).
7. S. Thiele, C. Pruss, A. M. Herkommer, and H. Giessen, "3D printed stacked diffractive microlenses," Opt. Express **27**(24), 35621–35630 (2019).
8. J. K. Hohmann, M. Renner, E. H. Waller, and G. von Freymann, "Three-dimensional μ-printing: an enabling technology," Adv. Opt. Mater. **3**(11), 1488–1507 (2015).
9. K. Weber, Z. Wang, S. Thiele, A. Herkommer, and H. Giessen, "Distortion-free multi-element Hypergon wide-angle micro-objective by femtosecond 3D printing," Opt. Lett. **45**(10), 2784–2787 (2020).
10. Z. Ma, X. Hu, Y. Zhang, X. Liu, Z. Hou, L. Niu, L. Zhu, B. Han, Q. Chen, and H.-B. Sun, "Smart compound eyes enable tunable imaging," Adv. Funct. Mater. **29**(38), 1903340 (2019).
11. R. Guo, S. Xiao, X. Zhai, J. Li, A. Xia, and W. Huang, "Micro lens fabrication by means of femtosecond two photon photopolymerization," Opt. Express **14**(2), 810–816 (2006).
12. G. Von Freymann, A. Ledermann, M. Thiel, I. Staude, S. Essig, K. Busch, and M. Wegener, "Three-dimensional nanostructures for photonics," Adv. Funct. Mater. **20**(7), 1038–1052 (2010).
13. T. Gissibl, S. Thiele, A. Herkommer, and H. Giessen, "Two-photon direct laser writing of ultracompact multi-lens objectives," Nat. Photonics **10**(8), 554–560 (2016).
14. A. Žukauskas, M. Malinauskas, and E. Brasselet, "Monolithic generators of pseudo-nondiffracting optical vortex beams at the microscale," Appl. Phys. Lett. **103**(18), 181122 (2013).
15. H. E. Williams, D. J. Freppon, S. M. Kuebler, R. C. Rumpf, and M. A. Melino, "Fabrication of three-dimensional micro-photonic structures on the tip of optical fibers using SU-8," Opt. Express **19**(23), 22910–22922 (2011).
16. P.-I. Dietrich, M. Blaicher, I. Reuter, M. Billah, T. Hoose, A. Hofmann, C. Caer, R. Dangel, B. Offrein, U. Troppenz, M. Moehrle, W. Freude, and C. Koos, "In situ 3D nanoprinting of free-form coupling elements for hybrid photonic integration," Nat. Photonics **12**(4), 241–247 (2018).
17. L. Jonušauskas, D. Gailevičius, L. Mikoliūnaitė, D. Sakalauskas, S. Šakirzanovas, S. Juodkazis, and M. Malinauskas, "Optically clear and resilient free-form μ-optics 3D-printed via ultrafast laser lithography," Materials **10**(1), 12 (2017).
18. N. Sultanova, S. Kasarova, and I. Nikolov, "Dispersion proper ties of optical polymers," Acta Phys. Pol., A **116**(4), 585–587 (2009).
19. S. Dottermusch, D. Busko, M. Langenhorst, U. W. Paetzold, and B. S. Richards, "Exposure-dependent refractive index of Nanoscribe IP-Dip photoresist layers," Opt. Lett. **44**(1), 29–32 (2019).
20. T. Gissibl, S. Wagner, J. Sykora, M. Schmid, and H. Giessen, "Refractive index measurements of photo-resists for three-dimensional direct laser writing," Opt. Mater. Express **7**(7), 2293–2298 (2017).
21. M. Schmid, D. Ludescher, and H. Giessen, "Optical properties of photoresists for femtosecond 3D printing: refractive index, extinction, luminescence-dose dependence, aging, heat treatment and comparison between 1-photon and 2-photon exposure," Opt. Mater. Express **9**(12), 4564–4577 (2019).
22. S. Steenhusen, F. Burmeister, H.-C. Eckstein, and R. Houbertz, "Two-photon polymerization of hybrid polymers for applications in micro-optics," in *Laser 3D Manufacturing II* (International Society for Optics and Photonics, 2015), Vol. 9353, p. 93530 K.
23. D. Werdehausen, S. Burger, I. Staude, T. Pertsch, and M. Decker, "Dispersion-engineered nanocomposites enable achromatic diffractive optical elements," Optica **6**(8), 1031–1038 (2019).
24. D. Werdehausen, I. Staude, S. Burger, J. Petschulat, T. Scharf, T. Pertsch, and M. Decker, "Design rules for customizable optical materials based on nanocomposites," Opt. Mater. Express **8**(11), 3456–3469 (2018).
25. C. Lü and B. Yang, "High refractive index organic–inorganic nanocomposites: design, synthesis and application," J. Mater. Chem. **19**(19), 2884–2901 (2009).
26. W. T. Doyle, "Optical properties of a suspension of metal spheres," Phys. Rev. B **39**(14), 9852–9858 (1989).
27. P. Tao, Y. Li, A. Rungta, A. Viswanath, J. Gao, B. C. Benicewicz, R. W. Siegel, and L. S. Schadler, "TiO2 nanocomposites with high refractive index and transparency," J. Mater. Chem. **21**(46), 18623 (2011).
28. Y. Imai, A. Terahara, Y. Hakuta, K. Matsui, H. Hayashi, and N. Ueno, "Transparent poly (bisphenol A carbonate)-based nanocomposites with high refractive index nanoparticles," Eur. Polym. J. **45**(3), 630–638 (2009).
29. V. A. Markel, "Introduction to the Maxwell Garnett approximation: tutorial," J. Opt. Soc. Am. A **33**(7), 1244–1256 (2016).
30. G. Mie, "Beiträge zur Optik trüber Medien, speziell kolloidaler Metallösungen," Ann. Phys. **330**(3), 377–445 (1908).
31. C. F. Bohren and D. R. Huffman, *Absorption and Scattering of Light by Small Particles* (John Wiley & Sons, 2008).
32. Pixelligent, "Application Notes: PixClear in ETA," http://www.pixelligent.com/wp-content/files/2016/07/Application-Note-PixClear-ETA-4pack-Rev003.pdf

Optical Materials EXPRESS

33. M. Shawer, E. Phillips, and M. J. Coffey, "Ophthalmic suspension composition," U.S. patent US20160213609A1 (2016).
34. S. T. Monickam, D. Peters, G. Cooper, and Z. Chen, "Nanocomposite formulations for optical applications," U.S. patent WO 2017/023642A1 (2017).
35. W. Xu, S. T. Monickam, J.-O. Choi, X. Bai, L. Gou, Z. S. Gonen-Williams, Z. Chen, and G. D. Cooper, "High refractive index nanocomposite," U.S. patent US 2014/0322549A1 (2014).
36. J. Guild, "Notes on the Pulfrich Refractometer," Proc. Phys. Soc. London **30**(1), 157–189 (1917).
37. D. L. Wood and K. Nassau, "Refractive index of cubic zirconia stabilized with yttria," Appl. Opt. **21**(16), 2978–2981 (1982).
38. W. T. Welford, *Aberrations of Optical Systems* (CRC Press, 1986).
39. D. Werdehausen, S. Burger, I. Staude, T. Pertsch, and M. Decker, "General design formalism for highly efficient flat optics for broadband applications," Opt. Express **28**(5), 6452–6468 (2020).
40. D. Werdehausen, S. Burger, I. Staude, T. Pertsch, and M. Decker, "Flat optics in high numerical aperture broadband imaging systems," J. Opt. **22**, 065607 (2020).
41. P. P. D. Kondiah, Y. E. Choonara, P. J. Kondiah, T. Marimuthu, P. Kumar, L. C. du Toit, G. Modi, and V. Pillay, "Nanocomposites for therapeutic application in multiple sclerosis," in *Applications of Nanocomposite Materials in Drug Delivery* (Elsevier, 2018), pp. 391–408
42. N. Dhas, K. Parekh, A. Pandey, R. Kudarha, S. Mutalik, and T. Mehta, "Two dimensional carbon based nanocomposites as multimodal therapeutic and diagnostic platform: A biomedical and toxicological perspective," *J. Control. Release* (2019).
43. G. Sandri, M. C. Bonferoni, S. Rossi, F. Ferrari, C. Aguzzi, C. Viseras, and C. Caramella, "Clay minerals for tissue regeneration, repair, and engineering," in *Wound Healing Biomaterials* (Elsevier, 2016), pp. 385–402.
44. Weber C. D., I. Edward, W. Elliott, J. P. Harmon, and G. Williams, "Inks for 3d printing gradient refractive index (grin) optical components," U.S. patent US20180022950A1 (2017).
45. C. D. Weber, C. G. Dupuy, J. P. Harmon, and D. M. Schut, "Inks for 3D printing gradient refractive index (GRIN) optical components," U.S. patent US9771490B2 (2016).